Type of the Paper (Article, Review, Communication, etc.)

On the slope stability of the submerged trench of the immersed tunnel subjected to solitary wave

Weiyun Chen[1,2], Dan Wang[1], Lingyu Xu[1], Zhenyu Lv[1], Zhihua Wang[1,*]

[1] *Institute of Geotechnical Engineering, Nanjing Tech University, Nanjing 210009, China*
[2] School of Civil Engineering, Sun Yat-Sen University, Guangzhou, 510275, China
* Correspondence: wzhnjut@163.com;

Abstract: Wave is a common environmental load that often causes serious damages to offshore structures. In addition, the stability for the submarine artificial slope is also affected by the wave loading. Although the landslide of submarine slopes induced by the waves has received wide attention, the research on the influence of solitary-wave is rare. In this study, a 2-D integrated numerical model is developed to investigate the stability of the foundation trench under the solitary wave loading. The Reynolds-Averaged-Stokes (RANS) equations are used to simulate the propagation of a solitary wave, while the current is realized by setting boundary inlet/outlet velocity. The pore pressure induced by the solitary wave is calculated by Darcy's law and the seabed is characterized by Mohr-Coulomb constitutive model. Firstly, the wave model is validated through the comparison between analytical solution and experimental data. The initial consolidation state of slope under hydrostatic pressure is achieved as the initial state. Then, the factor of stability (FOS) for the slope corresponding to different distance between wave crest and slope top is calculated with the strength reduction method. The minimum of FOS is defined as the stability index for the slope with specific slope ratio during the process of dynamic wave loading. The parametric study is conducted to examine the effects of soil strength parameters, slope ratio and current direction. At last, the influence of upper slope ratio in a two-stage slope is also discussed.

Keywords: Slope stability; Immersed tunnel; Solitary wave; foundation trench; numerical modeling

1. Introduction

With the continuous breakthrough of key technologies in the tunnel construction, underwater tunnel has gradually become an important means to cross rivers, lakes and seas. The immersed tube tunnel has been widely used in the submarine constructions for its advantages of being suitable for soft ground, short construction period and saving engineering cost. In general, the excavation of underwater foundation trench forms the temporary underwater slope, the stability of which has a significant impact on the safety of the whole construction.

The stability of foundation under different environment conditions has always been a crucial issue in the design of offshore structures. Seismic load and wave load are two common types of marine environment loading. The effects of seismic load acting on the seabed or offshore structure has attracted a lot of attention in the past decades[1-4]. Although the wave load is more common compared with the seismic action, the attention paid on the submarine slope under wave loading is not enough. A significant change in the pore pressure is induced in the seabed as the propagation of wave. The pressure exerted on the slope increases under the wave crest and it may result in significant displacements of slope [5]. Even if the artificial slope is temporary, its stability under wave loading needs to be guaranteed until the end of the construction. To make the slope construction both economic and ecologic, the volume of earth excavation should be as small as possible on the premise of stability[6].

Wave-induced responses in the seabed and offshore structures have been widely studied. Some analytical studies have been performed to investigate the changes of the wave-induced pore pressure and stresses in seabed [7-10]. Liu et al. [11] carried out an experimental study of wave-induced pore pressures in marine sediments and discussed the influences of parameters of wave and soil on the wave-induced liquefaction. Zhang et al. [12] developed a 3-D finite element method (FEM) model to simulate wave-induced response and considered the non-homogeneous soil properties. Considering the engineering applications, many investigations on the interaction between waves, seabed and structures have been conducted [13-18]. However, few studies have addressed the issue related to the slope stability of temporary foundation trench for the immersed tunnel under wave loading. Most of the existing works are concentrated on the regular linear waves such as progressive waves, neglecting the nonlinear waves [36].

Solitary wave is a kind of nonlinear wave often used to model the leading waves of storm surges such as tsunami in many studies [19-21]. In addition, the wave often take on the form of solitary wave near the shore in the shallow water, thus solitary wave is often used to model the behavior of the leading wave of storm surges. Concerning the interaction between solitary waves and coastal structures, some researches focused on the processes of solitary wave running up and running down on a uniform slope. Synolakis [22] measured the free wave surface of solitary wave on slope through the experiment. Summer et al. [23] conducted two parallel experiments of the solitary wave running up, breaking and falling on the sloping seabed and measured the shear stresses and pore water pressure. Young et al. [24] used the numerical method to predict liquefaction failure probability of slope on sandy coast caused by solitary waves and obtained the distribution of transient pressure, displacement and subsurface pore water pressure in the slope. Based on this, Xiao et al. [25] further investigated on the parameters that affect the maximum liquefaction depth, such as soil permeability, cross-shore location and offshore wave heights. Although the aforementioned studies concentrated mainly on the offshore slopes, the research on the stability of the artificial slope subjected to the solitary wave is still rare.

The objective of this study is to investigate the foundation trench for the immersed tunnel under the solitary wave loading based on a two-dimensional (2D) integrated model. The Reynolds-Averaged Navier-Stokes (RANS) equations combined with k-ε turbulence are adopted to simulate the solitary wave. The current is realized by setting boundary inlet and outlet velocity. In order to assess the stability index of the elastic-plastic slope, Darcy's law and Mohr-Coulomb yield criteria is used for the calculation of pore pressure. With the wave model verified, the dynamic response and specific failure mode of trench slope are then analyzed. Discussion on the effects of soil strength parameters, slope ratio and current direction on the slope is carried out through parametric studies. Considering that the trench slopes in practical engineering are often the slope with two stages or more stages, the influence of the upper slope ratio on the whole two-stage slope is investigated at last.

2. Theoretical formulations

The model consists of two sub-models: a wave-current model and a seabed model. The sketch of the numerical model for an artificial submarine slope under the combined action of current and solitary wave is shown in Fig.1. x and z are the Cartesian coordinates, h is the thickness of seabed, h_1 is the thickness of soil layer 1, h_2 is the thickness of soil layer 2, H is the height of solitary wave, W is the width of the trench, B is the height of the trench, d is the water depth and U_0 is the initial current velocity.

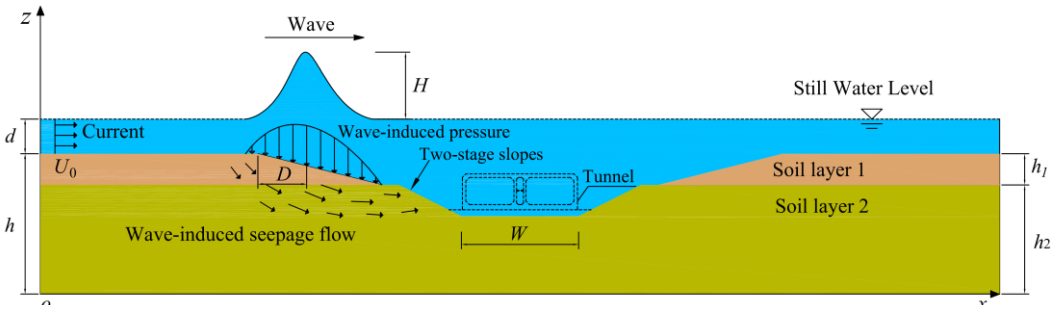

Figure 1. The solitary wave-artificial submarine slope coupling model

2.1 Wave-current sub-model

In this study, FLOW-3D which uses the finite difference method to solve the Navier-Stokes equation is adopted to simulate the propagation of solitary wave. The free surface motion is computed with a true volume of fluid (VOF) method [26,27] and the complex geometric regions is modeled by the fractional area/volume obstacle representation (FAVOR) technique [28].

2.1.1 Continuity equations and momentum equations

The flow is assumed to be incompressible and viscous fluid, the continuity equation in Cartesian coordinates can be expressed as:

$$\frac{\partial}{\partial x}(uA_x)+\frac{\partial}{\partial y}(vA_y)+\frac{\partial}{\partial z}(wA_z)=0 \tag{0}$$

where (u, v, w) are the velocity components in the coordinate direction (x, y, z); A_x, A_y and A_z are the fractional areas open to flow in the x, y and z directions.

The momentum equations of motion for the fluid velocity components (u, v, w) in the three coordinate directions are the Navier-Stokes (N-S) equations with some additional terms. The general N-S equations are described as:

$$\begin{aligned}
&\frac{\partial u}{\partial t}+\frac{1}{V_F}\{uA_x\frac{\partial u}{\partial x}+vA_y\frac{\partial u}{\partial y}+wA_z\frac{\partial u}{\partial z}\}=-\frac{1}{\rho}\frac{\partial p}{\partial x}+G_x+f_x\\
&\frac{\partial v}{\partial t}+\frac{1}{V_F}\{uA_x\frac{\partial v}{\partial x}+vA_y\frac{\partial v}{\partial y}+wA_z\frac{\partial v}{\partial z}\}=-\frac{1}{\rho}\frac{\partial p}{\partial y}+G_y+f_y\\
&\frac{\partial w}{\partial t}+\frac{1}{V_F}\{uA_x\frac{\partial w}{\partial x}+vA_y\frac{\partial w}{\partial y}+wA_z\frac{\partial w}{\partial z}\}=-\frac{1}{\rho}\frac{\partial p}{\partial z}+G_z+f_z
\end{aligned} \tag{0}$$

where V_F is the fractional volume open to flow; p is the water pressure; ρ is the fluid density; (G_x,G_y,G_z) are the body accelerations, (f_x,f_y,f_z) are the viscous accelerations.

2.1.2 Turbulence models

The $k-\varepsilon$ model has been demonstrated to provide reasonable approximations for various types of flows [29]. It consists of two transport equations for the turbulent kinetic energy k_T and its dissipation ε_T [30] .

The two transport equations are as follows:

$$\frac{\partial k}{\partial t}+\frac{\partial(uk)}{\partial x}+\frac{\partial(vk)}{\partial y}=\frac{\partial}{\partial x}[(\frac{\mu+\mu_t}{\sigma_k})\frac{\partial k}{\partial x}]+\frac{\partial}{\partial y}[(\frac{\mu+\mu_t}{\sigma_k})\frac{\partial k}{\partial y}]+G-\varepsilon \tag{0}$$

$$\frac{\partial \varepsilon}{\partial t}+\frac{\partial(u\varepsilon)}{\partial x}+\frac{\partial(v\varepsilon)}{\partial y}=\frac{\partial}{\partial x}[(\frac{\mu+\mu_t}{\sigma_\varepsilon})\frac{\partial \varepsilon}{\partial x}]+\frac{\partial}{\partial y}[(\frac{\mu+\mu_t}{\sigma_\varepsilon})\frac{\partial \varepsilon}{\partial y}]-C_{\varepsilon 1}\frac{\varepsilon^2}{k}G-C_{\varepsilon 2}\frac{\varepsilon^2}{k} \tag{0}$$

in which

$$\mu_t = C_\mu \frac{k^2}{\varepsilon} \tag{0}$$

$$G = \mu_t[(\frac{\partial u}{\partial y} + \frac{\partial v}{\partial x})^2 + 2(\frac{\partial u}{\partial x})^2 + 2(\frac{\partial v}{\partial y})^2] \tag{0}$$

where μ is the kinematic molecular viscosity; μ_t is kinematic eddy viscosity; k is the turbulent kinetic energy; ε is the turbulent kinetic energy dissipation rate; C_μ, $C_{\varepsilon 1}$, $C_{\varepsilon 2}$, σ_k and σ_ε are the empirical constants recommended in the literature [31]. The values in this study is as follows: C_μ=0.09, $C_{\varepsilon 1}$=1.44, $C_{\varepsilon 2}$=1.92, σ_k=1.0 and σ_ε=1.3.

2.1.3 Boundary conditions for solitary wave generation

In this model, the incident wave boundary is set at the left boundary to generate solitary wave, as shown in Fig. 1. The solitary wave solution is based on McCowan's theory [32] which has the higher order accuracy than Boussinesq's theory [33] and is recommended by Munk [34] after detailed examinations. The wave height is assumed to be H. The reference system (x, z) is established with its origin fixed at the bottom. A current exists and its x-component of undisturbed velocity is $\bar{u}$. The equations for water elevation η, x-velocity u, z-velocity w, and wave speed c are [34]:

$$\frac{\eta}{d} = \frac{N}{M} \frac{\sin[M(1+\frac{\eta}{d})]}{\cos[M(1+\frac{\eta}{d})] + \cosh(M\frac{X}{d})} \tag{0}$$

$$\frac{u(x,z,t)-\bar{u}}{c_0} = N \frac{1+\cos(\frac{Mz}{d})\cosh(\frac{MX}{d})}{[\cos(\frac{Mz}{d}) + \cosh(\frac{MX}{d})]^2} \tag{0}$$

$$\frac{w(x,z,t)}{c_0} = N \frac{\sin(\frac{Mz}{d})\sinh(\frac{MX}{d})}{[\cos(\frac{Mz}{d}) + \cosh(\frac{MX}{d})]^2} \tag{0}$$

$$c = \bar{u} + c_0 \tag{0}$$

where $c_0 = \sqrt{g(d+H)}$ is the wave speed in still water; g is the absolute value of gravitational acceleration; $X = x - ct$; M and N satisfy

$$\varepsilon = \frac{N}{M}\tan[\frac{1}{2}M(1+\varepsilon)] \tag{0}$$

$$N = \frac{2}{3}\sin^2[M(1+\frac{2}{3}\varepsilon)] \tag{0}$$

where $\varepsilon = H/d$.

The initial estimates of M and N are $M = \sqrt{3\varepsilon}$ and $N = 2\varepsilon$. The initial estimate of η is from Boussinesq's solution for solitary wave [33]

$$\frac{\eta}{d} = \varepsilon \operatorname{sech}^2(\sqrt{\frac{3\varepsilon}{4}}\frac{X}{d}) \quad \text{(initial estimate)} \tag{0}$$

2.2 Seabed sub-model

2.2.1 Seepage pressure

After the wave pressure is obtained from the wave model in Flow-3D, the seepage induced by the wave loading need to be calculated. In this study, the seepage pressure is calculated with Darcy's law. The seepage velocity can be affected by the factors such as pressure gradient, fluid viscosity and the structure of porous media, thus the Darcy's law can be expressed as:

$$u_s = -\frac{k_f}{\mu}\nabla p_s \tag{0}$$

where k_f is the permeability coefficient of porous seabed, μ is the dynamic viscosity of fluid, p_s is the seepage force, u_s is the seepage velocity in the seabed.

Combine the continuity equation with the Darcy's law, and the seepage pressure can be easily calculated under the solitary wave loading. The equation is as follows:

$$\frac{\partial}{\partial t}(\rho_w n) + \nabla(\rho_w u_s) = 0 \tag{0}$$

where ρ_w is the density of pore fluid, n is soil porosity.

2.2.2 Strength reduction method for the seabed

The seabed behavior is described by the Mohr-Coulomb constitutive model. Before determining the factor of safety (FOS) for the temporary slope formed by foundation trench excavation, the seepage pressure calculated by Darcy's law needs to be added to the total tensor of seabed. The shear stress in Mohr-Coulomb mechanical model can be expressed as

$$\tau_f = c' + \sigma_n \tan\varphi' \tag{0}$$

where c' and φ' are the effective cohesion and effective friction angle of the soil, respectively; σ_n is the normal stress.

It is assumed that the seabed material is isotropic and elastoplastic. The stability of the slope can be calculated by 2D plane strain approximation. With the Mohr-Coulomb yield criterion, the associated potential can be expressed as

$$F = m\sqrt{J_2} + \alpha_0 I_1 - k_0 \tag{0}$$

where F is the yield function, I_1 is the first invariant stress tensor, J_2 is the second invariant deviatoric stress tensor. m, α_0 and k_0 are the parameters related to soil material parameters:

$$m(\theta) = \cos(\theta - \pi/6) - \sqrt{1/3}\sin\varphi_{re}\sin(\theta - \pi/6), k_0 = c_{re}\cos\phi_{re} \tag{0}$$

where c_{re} and φ_{re} are the factored shear strength parameters which are defined as a function of *FOS* of slope [35].

$$c_{re} = \frac{1}{FOS}c' \tag{0}$$

$$\varphi_{re} = \arctan(\frac{1}{FOS}\tan\varphi') \tag{0}$$

The criterion to define the failure of slope is the non-convergence happening when the horizontal displacement increases dramatically in the process of calculation.

2.3 Boundary conditions

In order to get the accurate wave pressure, appropriate boundary conditions should be defined in the wave model at first. As shown in Fig. 1, the left side of the solitary wave model is the wave incident boundary, which is generated based on the solitary wave theory, and the inflow boundary is added at the same time to form the wave current inlet boundary; the right side of the solitary wave model is the wave outflow boundary with a wave-absorbing layer of 50m width; the upper boundary of the solitary wave model is the interface of water and air, and the air pressure is equal to a standard atmospheric pressure (101.3kPa); the bottom is the interface between water and soil and thus the wall boundary is adopted. The normal velocity of fluid on the boundary is zero.

In the seabed model, the pore pressure induced by the solitary wave is equal to the pressure obtained from the wave-current model at the surface of the seabed. At seabed surface, the boundary is described as:

$$p_s = p_b \tag{0}$$

where p_b is the pressure at seabed surface in the wave-current model.

The bottom and both sides of the seabed are set to be impermeable, furthermore, there is no horizontal displacement, which can be expressed as

$$\vec{n} \cdot \vec{u} = 0 \tag{0}$$

$$u_s = 0 \tag{0}$$

2.4 Integration of sub-models

In this study, the so-called one-way coupling method is adopted to realize the integration of wave-current sub-model and seabed sub-model. FDM (finite differential method) is used to solve the RANS equations in the wave-current sub-model, while FEM (finite element method) is used to calculate the seepage pressure and the seabed response. The size of the wave-current model is 200m×50m and the whole wave domain is divided into 5,024,294 cells with the cell size of 0.1m×0.1m. The aim of this model is to capture the wave-current pressure acting on the seabed, and then apply it to the surface in the seabed sub-model. The seabed sub-model is divided into triangular meshes with the maximum size of 2.81m and the minimum size of 0.025m. The mesh near the foundation trench is refined to make the calculation more accurately.

3. Model validation

To validate the calculation accuracy of the solitary wave pressure, the results of the wave model are compared with the laboratory experiments of Synolakis [22], in which a series of experiments about the process of solitary wave running up on the slope with the gradient of 1:19.85 were performed. One of the experiments was conducted with the wave height up to H/d = 0.3 and the maximum water depth d of 1m. The corresponding wave parameters are set the same as Synolakis [22], and the wave elevation is obtained at different time. Fig. 2 shows the comparison between the measured free water surface and the present model results. It is apparent that the process of the wave running up, down and breaking in the experiment is in good agreement with the current model, and thus the wave model is reliable.

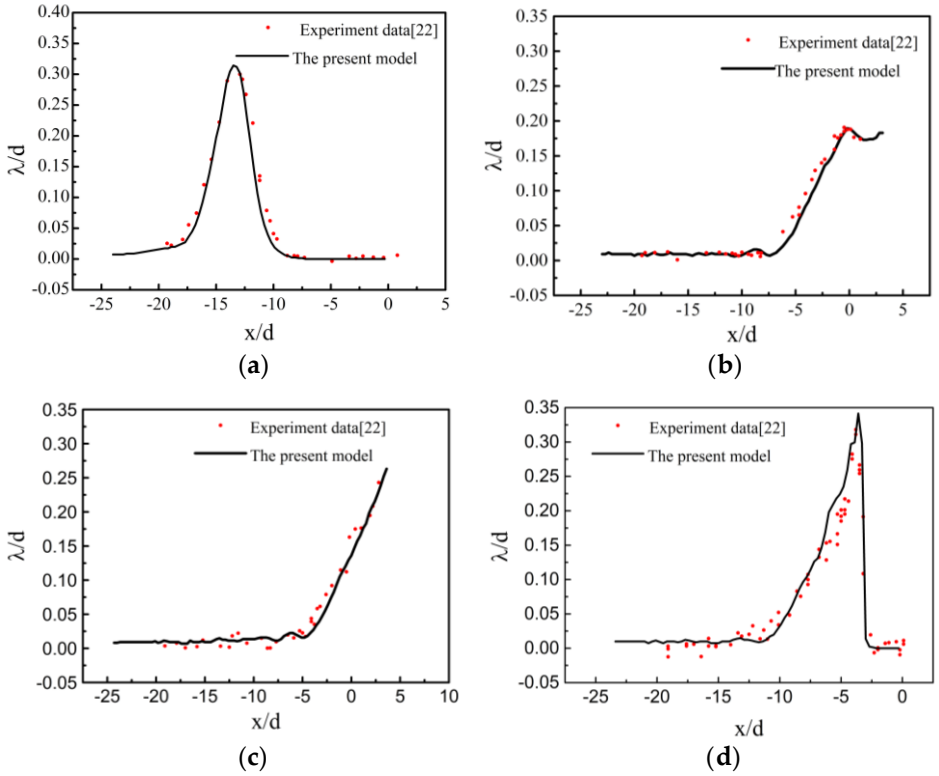

Figure 2. Comparison of wave surface profile between the proposed model and the experimental data [22]: (**a**) t = 10 s, (**b**) t = 20 s, (**c**) t = 25 s, (**d**) t = 30 s.

4. Results and discussion

4.1 Consolidation of the seabed

In general, the natural seabed has a consolidation process due to the existence of self-weight. The seabed will reach a new stable state of consolidation after being disturbed by the excavation of the foundation trench. Before adding the wave-induced pressure to the seabed, the state of stress and strain after the adequate reconsolidation under the hydrostatic pressure and self-gravity is determined. The calculation parameters are listed in Table.1. The width of the trench bottom (W) and vertical height of slope (B) are 34m and 18m, respectively. Fig. 3 shows the distribution of the stress and displacement in the foundation trench after reconsolidation, which is set as the initial condition for the model.

Table 1. Input parameters for parametric study.

Characteristics	Value	Unit
Wave parameters		
Wave height (H)	3	m
Water depth (d)	10	m
Soil parameters		
Seabed thickness (h)	40.5	m
Shear modulus (G)	6.56×10^{6}	Pa
Soil porosity (n)	0.41	
Poison's ratio (μ)	0.35	
Elastic modulus (E)	1.77×10^{7}	Pa
Soil permeability (k)	8×10^{-6}	m/s
Density of soil grain (ρ_s)	2.71×10^{3}	kg/m^3
Effective cohesion (c')	15	kPa
Effective internal friction angle (φ')	20	°
Trench width (W)	34	m

Trench height (B)	18	m
Water parameters		
Bulk modulus (K_w)	2×10^9	Pa
Density of water (ρ_w)	1000	kg/m^3

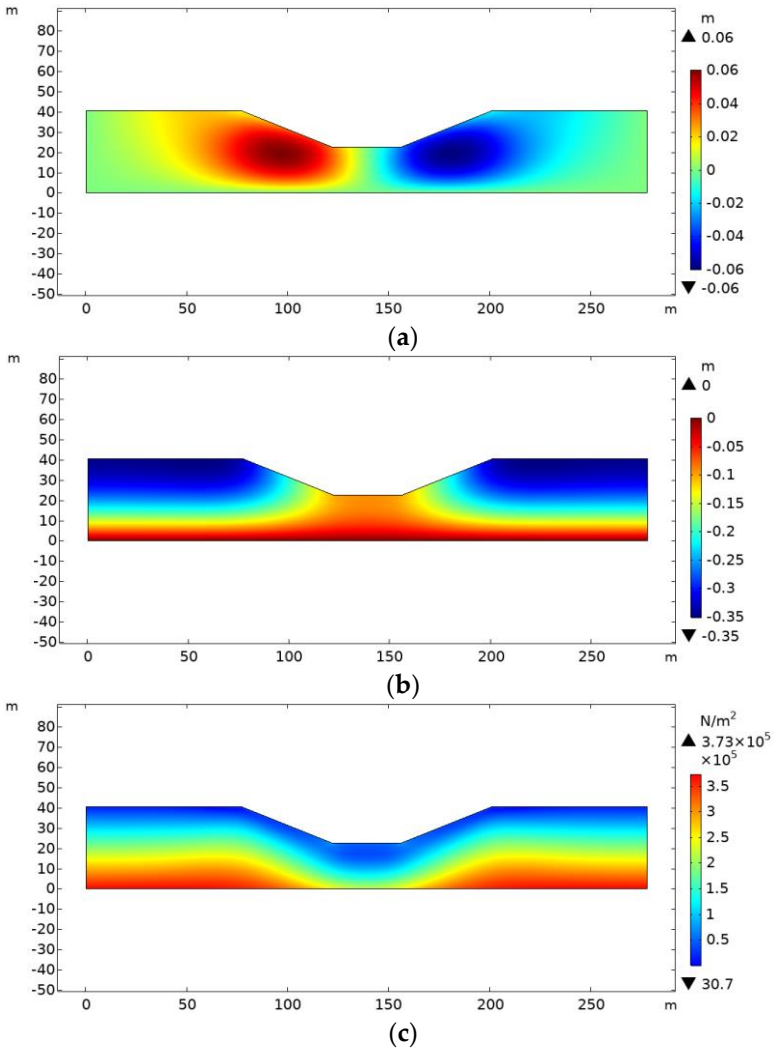

Figure 3. Initial state of the trench after excavation: (**a**) horizontal displacement, (**b**) vertical displacement, (**c**) stress state.

4.2 Stability index for the one-stage slope under solitary wave loading

To find the most dangerous moment in the whole process of solitary wave passing over the foundation trench, the stability indexes of the slope at different moments could be continuously calculated [36]. At different positions of the wave crest relative to the slope top from far to near, the factors of safety (FOS) for the slope are obtained correspondingly. The smallest FOS corresponds to the most dangerous moment, and the cases of different slope ratios are investigated in this section.

Fig. 4 illustrates the variation of FOS with D for the foundation trench slope with different slope ratios. Here D is denoted as the relative distance between the wave crest and slope top. The FOS for the slope only under the hydrostatic pressure is also obtained for comparison. It is obvious that the wave loading can significantly reduce the stability of the underwater slope. As the solitary wave crest propagates over the slope, the FOS decreases at first and then increases. As a result, the minimum of FOS can be determined for the slope with different slope ratios. Thus the minimum of the FOS (defined as FOS$_{min}$) is regarded as the stability index for the slope with the corresponding slope ratio. It

is observed that FOS_{min} is smaller than 1 when slope ratio is 1:2.5 in this case. Therefore, when the slope ratio is greater than 1:2.5, the slope may lose its stability under the combine actions of self-weight, wave pressure and the induced seepage force in the seabed.

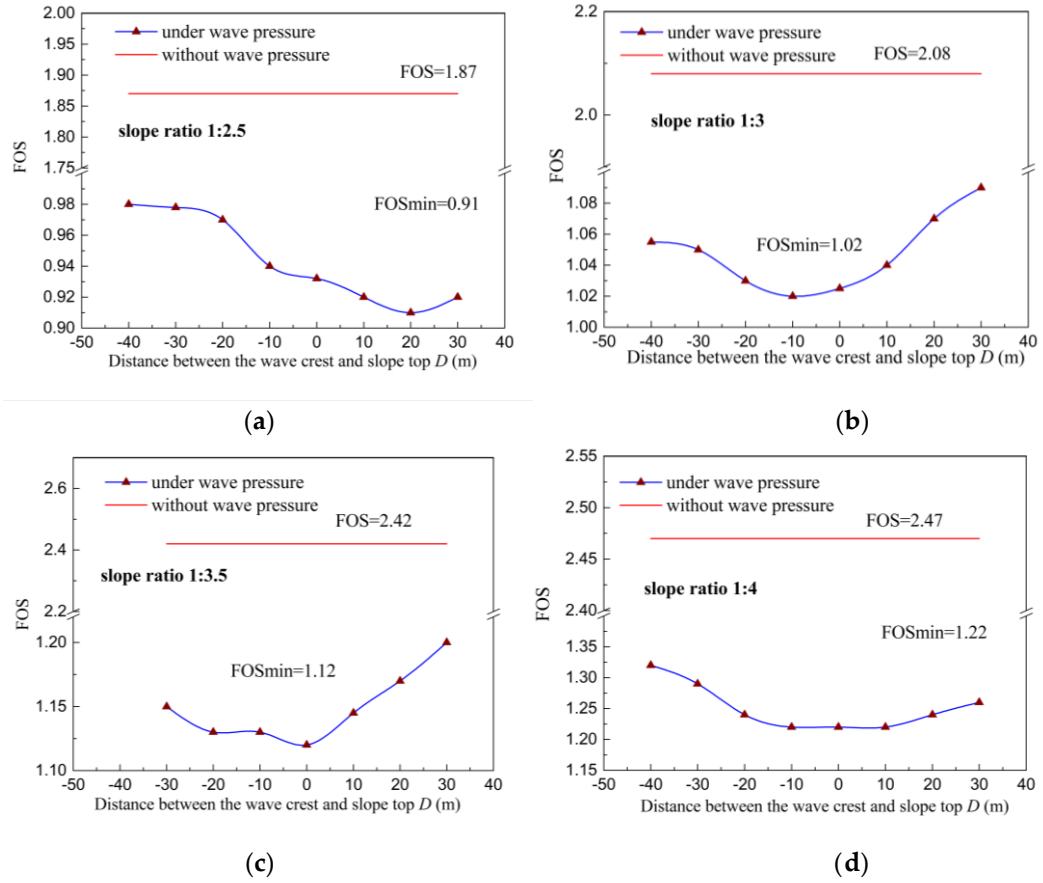

Figure 4. Variation of FOS with *D*: (**a**) slope ratio 1:2.5, (**b**) slope ratio 1:3, (**c**) slope ratio 1:3.5, (**d**) slope ratio 1:4.

4.3 Influence of soil strength parameters on the slope stability

Generally speaking, soil properties have a great influence on the wave-induced pore pressure and displacement in the slope. In this section, two important soil parameters, cohesion and internal friction angle, are discussed. The soil cohesion c' taken is taken to be 13kPa, 15kPa, 17kPa and 19kPa, respectively. While the internal friction angle φ' is taken to be 12°, 16°, 20°, and 24° respectively. Fig. 5 illustrates the influences of cohesion and internal friction on the displacement contour of 0.2m in the slope. It is noted that the increase of cohesion increases the failure depth and enlarges the area of landslide. With the increase of friction angle, the sliding damage area and failure depth decrease gradually. The results in this section agree well with that of the slopes on land in Cheng et al. [37].

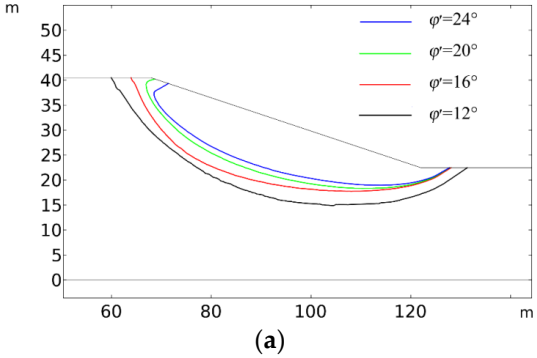

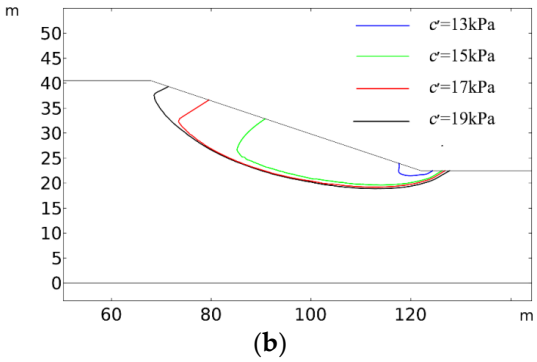

Figure 5. Destruction areas of the slope with different soil parameters: (a) φ'=24°, 20°, 16°, 12°; (b) c'=13kPa, 15kPa, 17kPa, 19kPa.

4.4 Influence of slope ratio on slope stability

The slope ratio of the trench directly affects the amount of excavation and backfilling materials, and thus has an important influence on the cost of trench excavation of immersed tunnel. Obviously, the larger the slope ratio is, the more stable the slope is. Since the stability is not the only one factor to be considered, reasonable slope ratio should be achieved to ensure the balance between economy and safety in practical project. The wave and soil parameters are chosen from Table 1. The slope rate is set to be 1:2, 1:2.5, 1:3, and 1:3.5, respectively. Fig. 6 demonstrates the distribution of equivalent plastic strain in four different cases in the seabed. When the plastic zone develops continuously through the toe to the top, the landslide is likely to happen. It is shown that the maximum plastic strain in the seabed increases with the increasing slope ratio, as expected.

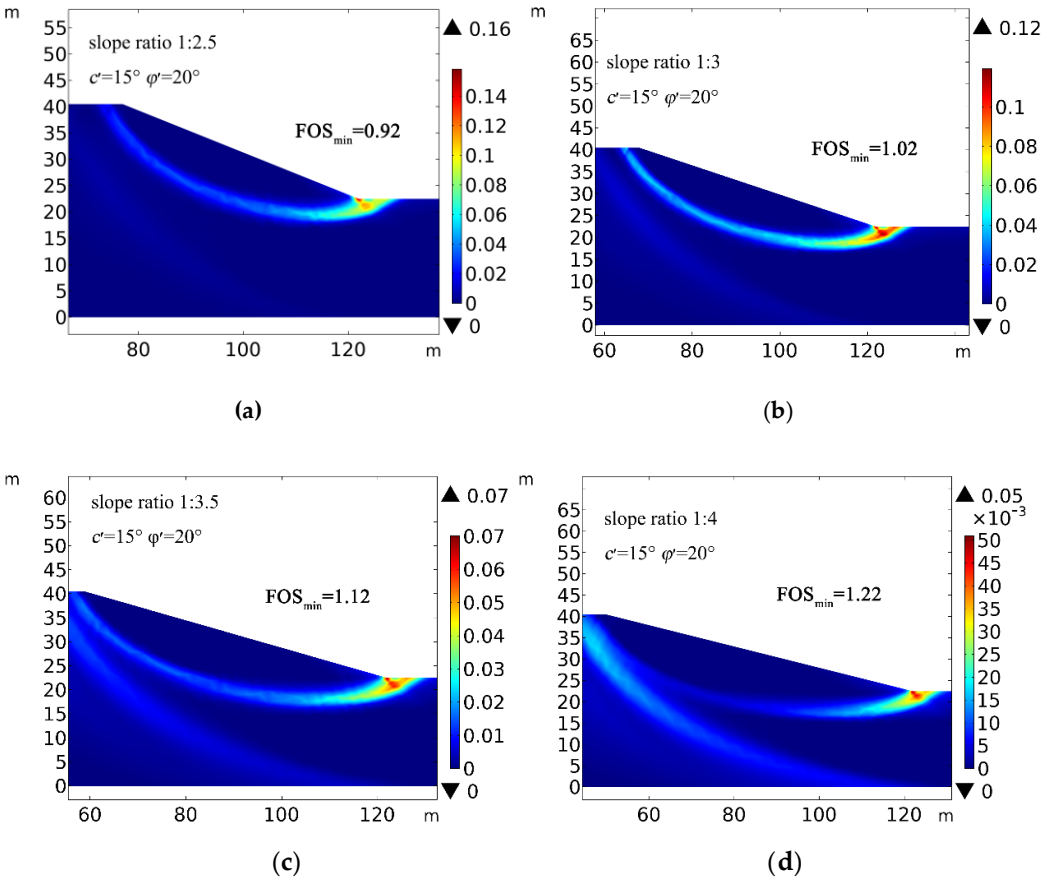

Figure 6. Plastic penetration zones in the slope with different slope rates: (**a**) slope rate 1:2.5, (**b**) slope rate 1:3, (**c**) slope rate 1:3.5, (**d**) slope rate 1:4.

Fig. 7 demonstrates the actual failure deformation for the slope with four slope ratios and the scale factor adopted is 1:20. The sliding area has an arc-shaped layered division. The maximum deformation of the slope occurs at the toe of the slope and has the tendency to concentrate at the bottom with the increasing of slope ratio.

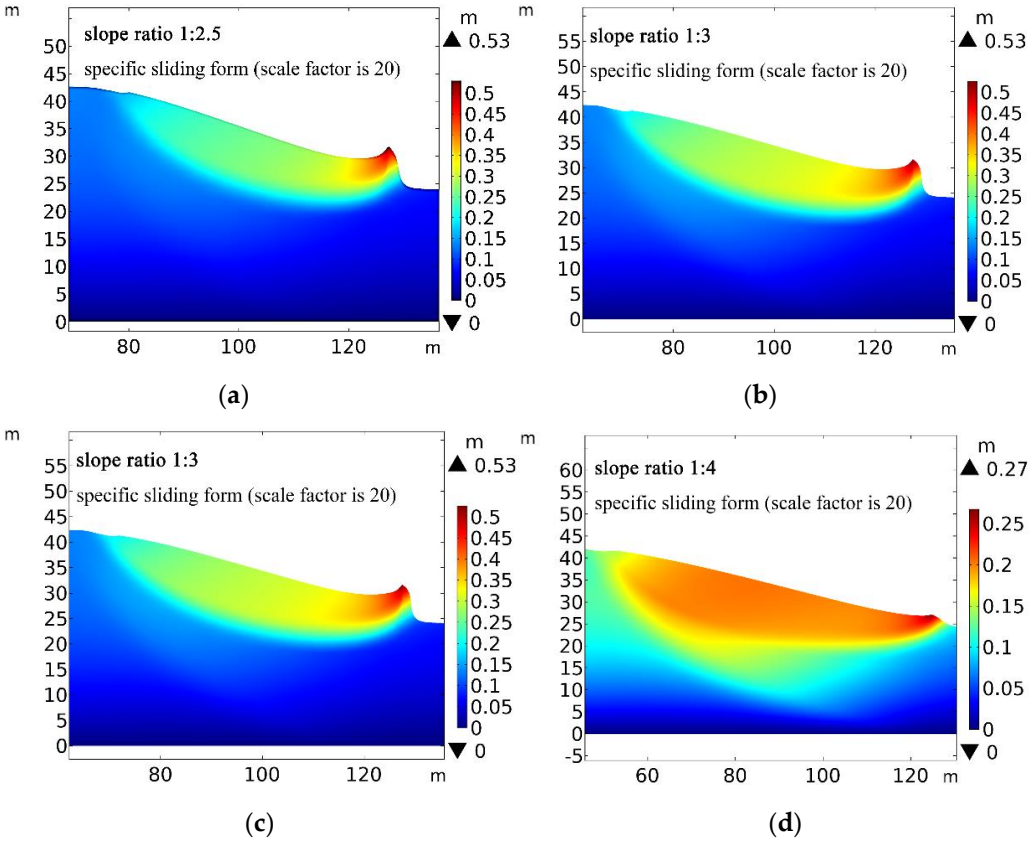

Figure 7. Sliding displacements in the slope with different slope rates (scale factor is 20): (a) slope ratio 1:2.5, (b) slope ratio 1:3, (c) slope ratio 1:3.5, (d) slope ratio 1:4.

4.5 Influence of current direction on slope stability

The current flow can affect the propagation of solitary wave, thus has further impact on the failure of the slope. In this section, two different current directions are discussed, one is the flow and current in the same direction (+1m/s, wave co-current) and the other is in the opposite direction (-1m/s, wave counter-current). The deformation of both sides of the slope is illustrated in Fig. 8, in which Figs. 8(a) and 8(b) are the left and right slope deformations in the case of wave co-current (+1m/s), while Figs. 8(c) and 8(d) are the left and right slope deformations in the cases of waves counter-current exists (-1m/s). It can be observed that the FOS_{min} in Figs. 8(a) and 8(d) are smaller than those in Figs. 8(b) and 8(c). This phenomenon may be attributed to the fact that when the currents propagate away from the slope surface, the current-induced pressure acting on the slope surface may reduce the stability of slope.

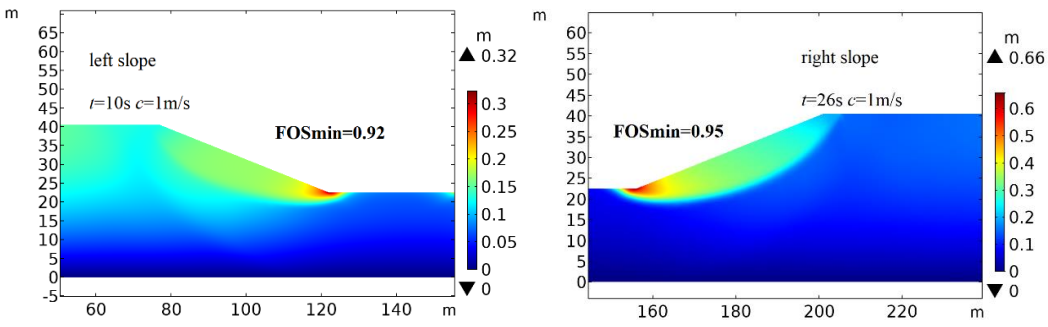

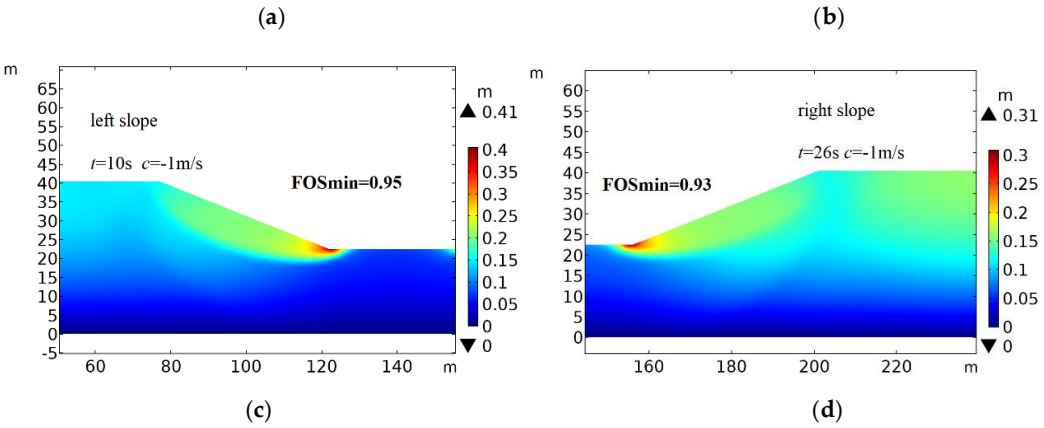

Figure 8. Deformation of the trench slopes under the currents in different directions: (a) left slope, 1m/s; (b) right slope, 1m/s; (c) left slope, -1m/s; (d) right slope, -1m/s.

4.6 Influence of slope ratio on two-stage slope

Table 2. Input soil parameters of the two-stage slope

Characteristics	Value	Unit
Soil parameters in upper slope		
Seabed thickness	8	m
Shear modulus	4.33×10^{6}	Pa
Soil porosity	0.56	
Poison's ratio	0.35	
Elastic modulus	1.17×10^{7}	Pa
Soil permeability	1×10^{-9}	m/s
Density of soil grain	2.75×10^{3}	kg/m^3
Effective cohesion	12	kPa
Effective internal friction angle	13	°
Soil parameters in lower slope		
Seabed thickness	32.5	m
Shear modulus	6.56×10^{6}	Pa
Soil porosity	0.41	
Poison's ratio	0.35	
Elastic modulus	1.77×10^{7}	Pa
Soil permeability	8×10^{-6}	m/s
Density of soil grain	2.71×10^{3}	kg/m3
Effective cohesion	15	kPa
Effective internal friction angle	20	°

Due to the uneven distribution of horizontal layers, two-stage slope is mostly used in the trench excavation in practical engineering [38]. In this section, the effects of the ratios of upper slope and lower slope on the stability of the two-stage trench slope are investigated. The heights of the upper and lower slopes are set be the same and the soil parameters for the lower and upper slopes are selected from Table. 2. The ratio of the lower slope is set to be 1:2, 1:2.5, and 1:3, respectively. Fig. 9 shows the variation of FOS_{min} with the ratio of upper slope. It can be noted that FOS_{min} firstly increases and then remain almost unchanged with the increase of the upper slope ratio in Figs. 9(a) and 9(b). When the lower slope ratio is 1:3, the FOS_{min} increases slightly as the upper slope ratio increases. Thus, it can be concluded that the ratio of the lower slope has more significant influence on the stability of the whole slope, compared with the upper slope.

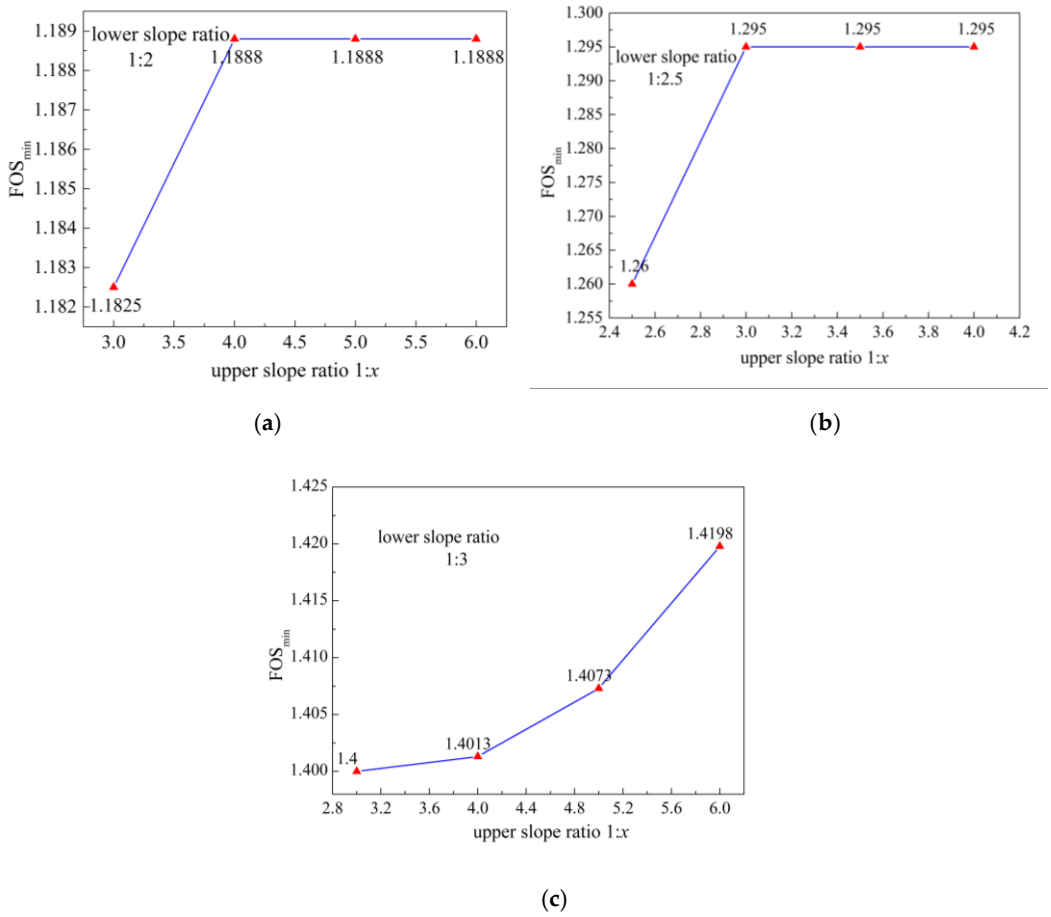

Figure 9. Variation of FOS_{min} with the ratio of upper slope with various lower slope ratios: (a) lower slope ratio 1:2, (b) lower slope ratio 1:2.5, (c) lower slope ratio 1:3.

5. Conclusions

In this study, an integrated numerical model is developed to investigate the potential for the failure of the foundation trench of the immersed tunnel under solitary wave loading. Darcy'law is adopted to calculate the pore water pressure and the soil behavior is described by the Mohr-Coulomb constitutive model. The strength reduction method is applied in investigating the stability index for the foundation trench under the dynamic wave loading. Based on the calculation, the following conclusions can be drawn:

(1) The factor of stability (FOS) for the slope varies as the relative distance between wave crest and the top of the slope changes. The wave motion can significantly affect the stability of the slope seabed foundation. The minimum of FOS corresponds to the most dangerous situation of the slope with specific slope ratio under the solitary wave loading.

(2) The soil strength parameters have great impact on the area and depth of the slope failure. The slope failure area and depth increase with the increase of soil cohesion, but decrease with the increase of internal friction angle.

(3) As the slope ratio increases, the FOS decreases, and the maximum deformation is more likely to concentrate at the toe of the slope with the increasing slope ratio.

(4) The FOS of the slope in the case that currents propagate towards the slope surface is greater than that in the case the currents propagate away from the slope surface. It is noted that the current propagating away from the slope could increase the possibility of slope instability.

(5) When the foundation trench takes the form of two-stage slope, the ratio of lower slope has more significant influence on the stability of the whole slope, compared with that of the upper slope.

Acknowledgments: The authors gratefully acknowledge the financial support provided by the National Natural Science Foundation of China (No. 41877243).

References

1. Chen, W.Y.; Wang, Z.H.; Chen, G.X.; Jeng, D.S.; Wu, M.; Zhao, H.Y. Effect of vertical seismic motion on the dynamic response and instantaneous liquefaction in a two-layer porous seabed. *Comput Geotech* **2018**, 99, 165-176.
2. Chen, W.Y.; Huang, Y.; Wang, Z.H.; He, R.; Chen, G.X.; Li, X.J. Horizontal and vertical motion at surface of a gassy ocean sediment layer induced by obliquely incident SV waves. *Eng Geol* **2017**, 227, 43-53.
3. Chen, G.X.; Ruan, B.; Zhao, K.; Chen, W.Y.; Zhuang, H.Y.; Du, X.L.; Khoshnevisan, S.; Juang, C.H. Nonlinear Response Characteristics of Undersea Shield Tunnel Subjected to Strong Earthquake Motions. *J Earthq Eng* **2020**, 24, 351-380.
4. Xu, L.Y.; Song, C.X.; Chen, W.Y.; Cai, F.; Li, Y.Y.; Chen, G.X. Liquefaction-induced settlement of the pile group under vertical and horizontal ground motions. *Soil Dyn Earthq Eng* **2021**, 144, 106709.
5. Henkel, D. The Role of Waves in Causing Submarine Landslides. *Geotechnique* **1970**, 20, 75-80.
6. Bubel, J.; Grabe, J. Stability of Submarine Foundation Pits Under Wave Loads, Asme International Conference on Ocean, Rio de Janeiro, Brazil, 2012; pp. 11.
7. Jeng, D.S. Wave-induced liquefaction potential at the tip of a breakwater: an analytical solution. *Appl Ocean Res* **1996**, 18, 229-241.
8. Madsen, O.S. Wave-induced pore pressures and effective stresses in a porous bed. *Géotechnique* **1978**, 28, 377-393.
9. Yamamoto, T. Wave-induced pore pressures and effective stresses in inhomogeneous seabed foundations. *Ocean Eng* **1981**, 8, 1-16.
10. Mei, C.C.; Foda, M.A. Wave-induced responses in a fluid-filled poro-elastic solid with a free surface—a boundary layer theory. *Geophys J Int* **1981**, 66, 597-631.
11. Liu, B.; Jeng, D.S.; Ye, G.L.; Yang, B. Laboratory study for pore pressures in sandy deposit under wave loading. *Ocean Eng* **2015**, 106, 207-219.
12. Zhang, C.; Titi, S.; Zheng, J.H.; Xie, M.X.; Nguyen, V.T. Modelling wave-induced 3D non-homogeneous seabed response. *Appl Ocean Res* **2016**, 61, 101-114.
13. Lin, Z.B.; Guo, Y.K.; Jeng, D.S.; Liao, C.C.; Rey, N. An integrated numerical model for wave–soil–pipeline interactions. *Coast Eng* **2016**, 108, 25-35.
14. Lin, Z.B.; Pokrajac, D.; Guo, Y.K.; Jeng, D.S.; Tang, T.; Rey, N.; Zheng, J.H.; Zhang, J.S. Investigation of nonlinear wave-induced seabed response around mono-pile foundation. *Coast Eng* **2017**, 121, 197-211.
15. Duan, L.L.; Liao, C.C.; Jeng, D.S.; Chen, L.Y. 2D numerical study of wave and current-induced oscillatory non-cohesive soil liquefaction around a partially buried pipeline in a trench. *Ocean Eng* **2017**, 135, 39-51.
16. Zhai, Y.Y.; He, R.; Zhao, J.L.; Zhang, J.S.; Jeng, D.S.; Li, L. Physical Model of wave-induced seabed response around trenched pipeline in sandy seabed. *Appl Ocean Res* **2018**, 75, 37-52.
17. Zhang, Q.; Zhou, X.L.; Wang, J.H.; Guo, J.J. Wave-induced seabed response around an offshore pile foundation platform. *Ocean Eng* **2017**, 130, 567-582.
18. Zhao, H.Y.; Zhu, J.F.; Zheng, J.H.; Zhang, J.S. Numerical modelling of the fluid–seabed-structure interactions considering the impact of principal stress axes rotations. *Soil Dyn Earthq Eng* **2020**, 136, 106242.
19. Lara, J.L.; Losada, I.J.; Maza, M.; Guanche, R. Breaking solitary wave evolution over a porous underwater step. *Coast Eng* **2011**, 58, 837-850.
20. Synolakis, C.E.; Bernard, E.N. Tsunami science before and beyond Boxing Day 2004. *Philosophical Transactions of the Royal Society A: Mathematical, Physical and Engineering Sciences* **2006**, 364, 2231-2265.
21. Hsiao, S.C.; Lin, T.C. Tsunami-like solitary waves impinging and overtopping an impermeable seawall: Experiment and RANS modeling. *Coast Eng* **2010**, 57, 1-18.
22. Synolakis, C.E. The runup of solitary waves. *J Fluid Mech* **1987**, 185, 523-545.
23. Sumer, B.M.; Sen, M.B.; Karagali, I.; Ceren, B.; Freds E, J.R.; Sottile, M.; Zilioli, L.; Fuhrman, D.R. Flow and sediment transport induced by a plunging solitary wave. *J Geophys Res* **2011**, 116, C1008.
24. Young, Y.L.; White, J.A.; Xiao, H.; Borja, R.I. Liquefaction potential of coastal slopes induced by solitary waves. *Acta Geotech* **2009**, 4, 17-34.
25. Xiao, H.; Young, Y.L.; Prévost, J.H. Parametric study of breaking solitary wave induced liquefaction of coastal sandyslopes. *Ocean Eng* **2010**, 37, 1546-1553.
26. Nichols, B.D.; Hirt, C.W.; Hotchkiss, R.S. SOLA-VOF: A solution algorithm for transient fluid flow with multiple free boundaries. *Tech. Rep. LA-8355* **1980**, 39.

27. Hirt, C.W.; Nichols, B.D. Volume of fluid (VOF) method for the dynamics of free boundaries. *J Comput Phys* **1981**, 39, 201-225.
28. Hirt, C.; Sicilian, J. A Porosity Technique for the Definition of Obstacles in Rectangular Cell Meshes, International Conference on Numerical Ship Hydrodynamics, 4th, Washington, DC, 1985-01-01, pp.19.
29. Launder, B. E.; Spalding, D. B. The numerical computation of turbulent flows. *Comput Method Appl M* **1974**, 3, 269-289.
30. Harlow, F.H.; Nakayama, P.I. Turbulence Transport Equations. *Phys Fluids* **1967**, 10, 2323-2332.
31. Franke, R.; Rodi, W. Calculation of Vortex Shedding Past a Square Cylinder with Various Turbulence Models, Berlin, Heidelberg, 1993-01-01, 1993; Durst, F.; Friedrich, R.; Launder, B.E.; Schmidt, F.W.; Schumann, U.; Whitelaw, J.H., Eds. Springer Berlin Heidelberg: Berlin, Heidelberg, pp. 189-204.
32. McCowan, J. VII. On the solitary wave. *The London, Edinburgh, and Dublin Philosophical Magazine and Journal of Science* **1891**, 32, 45-58.
33. Boussinesq, J.V. Theorie de L'intumescence Liguide Appelee onde Solitaire ou de Translation se Propageant dans un Canal Rectangulaire. In 1871; Vol. 72, pp. 755-759.
34. Munk, W.H. The solitary wave theory and its application to surf problems. *Ann Ny Acad Sci* **1949**, 51, 376-424.
35. Matsui, T.; San, K. Finite Element Slope Stability Analysis by Shear Strength Reduction Technique. *Soils Found* **1992**, 32, 59-70.
36. Chen, W.Y.; Liu, C.L.; Li, Y.; Chen, G.X.; Yu, J. An integrated numerical model for the stability of artificial submarine slope under wave load. *Coast Eng* **2020**, 158, 103698.
37. Cheng, Y.M.; Länsivaara, T.; Wei, W.B. Two-dimensional slope stability analysis by limit equilibrium and strength reduction methods. *Comput Geotech* **2007**, 34, 137-150.
38. Hu, Z.N.; Xie, Y.L.; Wang, J. Challenges and strategies involved in designing and constructing a 6 km immersed tunnel: A case study of the Hong Kong–Zhuhai–Macao Bridge. *Tunn Undergr Sp Tech* **2015**, 50, 171-177.